npj | Quantum Materials
www.nature.com/npjquantmats

ARTICLE OPEN

Observation of two superconducting domes under pressure in tetragonal FeS

Jun Zhang[1], Feng-Liang Liu[1,2], Tian-Ping Ying[1], Na-Na Li[2], Yang Xu[1], Lan-Po He[1], Xiao-Chen Hong[1], Yun-Jie Yu[1], Ming-Xiang Wang[1], Jian Shen[1,3], Wen-Ge Yang[2,4] and Shi-Yan Li[1,3]

We investigate the evolution of superconductivity and structure with pressure for the new superconductor FeS ($T_c \approx 4.5$ K), a sulfide counterpart of FeSe. A rapid suppression of T_c and vanishing of superconductivity at 4.0 GPa are observed, followed by a second superconducting dome from 5.0 to 22.3 GPa with a 30% enhancement in maximum T_c. An onsite tetragonal to hexagonal phase transition occurs around 7.0 GPa, followed by a broad pressure range of phase coexistence. The residual deformed tetragonal phase is considered as the source of second superconducting dome. The observation of two superconducting domes in iron-based superconductors poses great challenges for understanding their pairing mechanism.

npj Quantum Materials (2017)2:49 ; doi:10.1038/s41535-017-0050-7

INTRODUCTION

As the second family of high-T_c superconductor, the iron-based superconductors (IBSs) have been extensively studied in recent years.[1–3] Among those IBSs, the tetragonal FeSe with the simplest structure has attracted much attention recently.[4] Although the T_c of bulk FeSe is modestly low (≈8 K),[4] it can be enhanced through various methods. By applying high pressure, the T_c of bulk FeSe can reach up to 36.7 K.[5, 6] Through intercalation, surface K dosing, or ionic liquid gating, one can also enhance the T_c to above 40 K.[7–11] Surprisingly, the T_c can be further enhanced above 60 K by growing monolayer FeSe thin film on $SrTiO_3$ substrate,[12–16] and even above 100 K on Nb-doped $SrTiO_3$ substrate.[17] It was believed that the enhanced electron–phonon coupling at interface is crucial in the further enhancement of T_c.[18, 19]

The angle-resolved photoemission spectroscopy studies reveal two distinct electronic band structures for these FeSe-based superconductors. The Fermi surface of the undoped bulk FeSe consists of hole pockets around Γ and electron pockets around M.[15, 20–23] However, for intercalated $(Li_{0.8}Fe_{0.2})OHFeSe$, monolayer FeSe thin film, and surface K dosed FeSe single crystal or film, the Fermi surface consists of only electron pockets, which apparently results from electron doping.[7, 13–16, 24–27] For undoped bulk FeSe, the superconducting pairing symmetry is most likely $s\pm$-wave with sign reversal between the hole and electron pockets,[28] while for monolayer FeSe/$SrTiO_3$, plain *s*-wave superconductivity was suggested by scanning tunneling microscopy (STM) study.[29] Because of the large variety of FeSe-based superconductors with a wide range of T_c, clarifying the superconducting mechanism will be a major step towards solving the issue of high-temperature superconductivity in IBSs.

Very recently, superconductivity with $T_c \approx 4.5$ K at ambient pressure was reported for FeS,[30] the sister compound of FeSe. As an important Earth Science material, FeS has been extensively studied including high-pressure works,[31] but superconductivity had not been observed until high-quality stoichiometric tetragonal FeS was successfully synthesized by low-temperature hydrothermal method.[30] The tetragonal FeS has the same crystal structure as the tetragonal FeSe, and their electronic structures are also quite similar based on first principle calculation.[32] A slight difference between them is that FeSe undergoes a phase transition to orthorhombic structure at 90 K,[33] while FeS remains its tetragonal structure down to 10 K.[34] Interestingly, recent thermal conductivity and specific heat measurements suggested nodal superconductivity in FeS.[35, 36]

Here we present *in situ* high-pressure electrical transport and synchrotron X-ray diffraction (XRD) measurements on tetragonal FeS single crystals. Upon applying pressure, two superconducting domes are observed. The first dome manifests a continuous decrease of T_c with increasing pressure, ending ~4.0 GPa. Then a second superconducting dome emerges from 5.0 GPa and lasts to 22.3 GPa, with an over 30% increasing in T_c (≈6.0 K) from the highest T_c in the first dome. Comparing to the two superconducting domes of $(K/Tl/Rb)_xFe_{2-y}Se_2$ reported earlier,[37] the superconducting pressure range is much wider, meaning the superconducting phase is much more sustainable with pressure in FeS. For its crystal structure, a hexagonal phase starts to set in at ~7.0 GPa, and there is a large coexisting pressure range of tetragonal and hexagonal phases. On the basis of the drop in $R(T)$ curves and the structure refinement results of mixture phase region, we believe that the second superconducting dome is originated from the residual deformed tetragonal phase of FeS.

RESULTS

Characterization at ambient pressure

The inset of Fig. 1a is a photo of as-grown FeS single crystals. Figure 1a shows a typical XRD pattern, in which only the (00l)

[1]State Key Laboratory of Surface Physics, Department of Physics, and Laboratory of Advanced Materials, Fudan University, Shanghai 200433, China; [2]Center for High Pressure Science and Technology Advanced Research (HPSTAR), Shanghai 201203, China; [3]Collaborative Innovation Center of Advanced Microstructures, Nanjing 210093, China and [4]High Pressure Synergetic Consortium (HPSynC), Geophysical Laboratory, Carnegie Institution of Washington, Argonne, IL 60439, USA
Correspondence: Wen-Ge Yang (yangwg@hpstar.ac.cn) or Shi-Yan Li (shiyan_li@fudan.edu.cn)
Jun Zhang, Feng-Liang Liu and Tian-Ping Ying contributed equally to this work

Received: 2 November 2016 Revised: 2 July 2017 Accepted: 11 July 2017
Published online: 01 September 2017

npj nature partner journals

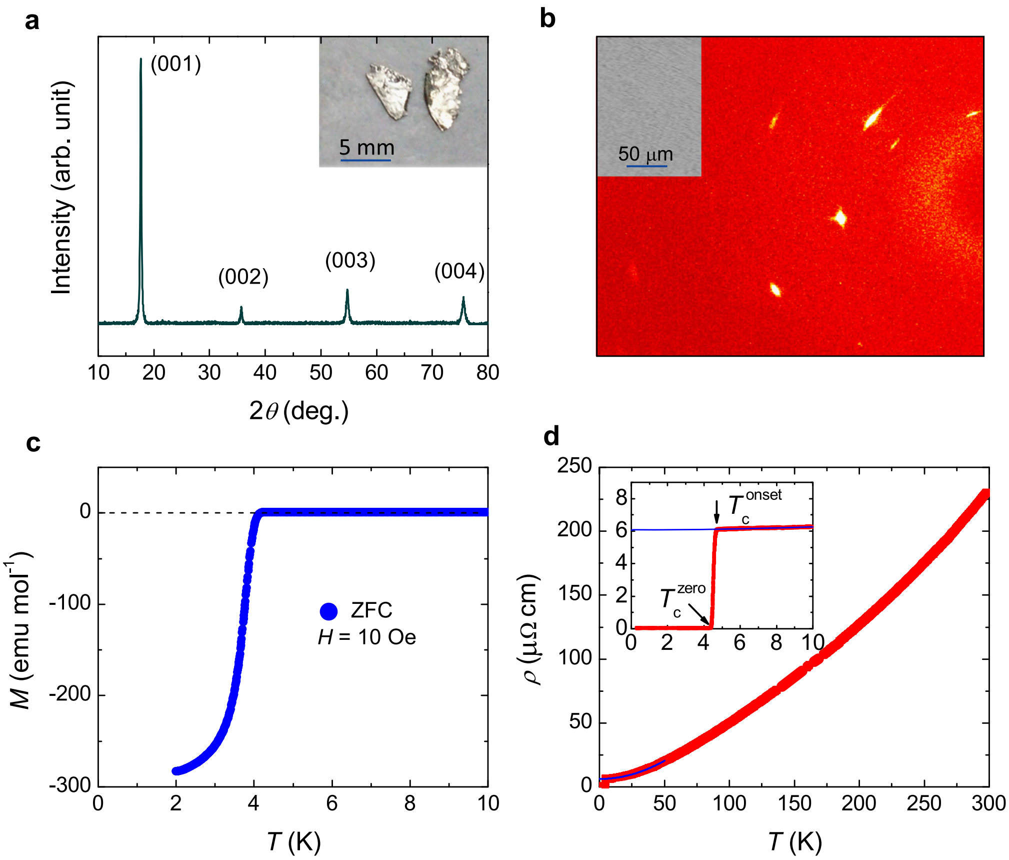

Fig. 1 **a** Typical XRD pattern of FeS single crystals. The inset shows a photo of the as-grown FeS single crystals. **b** Single crystal XRD spots of an FeS sample. The inset is an SEM image of the surface. **c** Low-temperature dc magnetization measured in the ZFC mode at $H = 10$ Oe parallel to the *c* axis. **d** Temperature dependence of the resistivity $\rho(T)$. The inset is an enlarged view of the superconducting transition. ZFC, zero-field-cooled

Bragg peaks show up, indicating the crystals are well oriented along the *c* axis. Further XRD measurement on these crystals shows sharp single crystal diffraction spots (Fig. 1b). Flat and grain-boundary-free surface was observed with SEM (inset of Fig. 1b). Therefore, the single crystalline nature of our FeS samples is confirmed.

Figure 1c shows a typical low-temperature dc magnetization of FeS single crystals, from which the superconducting transition is at ~4.1 K. The temperature dependence of resistivity $\rho(T)$ at ambient pressure is plotted in Fig. 1d. The absence of a resistivity anomaly in the normal state suggests no structural phase transition, which is different from FeSe single crystal.[33] The low-temperature resistivity between 5 and 50 K can be well described by the Fermi liquid theory, $\rho(T) = \rho_0 + AT^2$, giving $\rho_0 = 6.07$ μΩ cm and $A = 2.0 \times 10^{-3}$ μΩ cm/K^2. The residual resistivity ratio, RRR = ρ(298 K)/ $\rho_0 = 40$, is much larger than that reported previously for FeS flakes.[30] The inset of Fig. 1d displays an enlarged view around the superconducting transition, from which $T_c^{onset} \approx 4.7$ K and $T_c^{zero} \approx 4.3$ K are obtained. T_c^{onset} is determined as the temperature where the resistivity deviates from the normal-state behavior, while T_c^{zero} as the temperature where the resistivity drops to zero. In the following discussions, we use T_c^{onset} as T_c.

T_c evolution under pressure

The temperature dependence of resistance up to 4.0 GPa is plotted in Fig. 2a, where the resistance is normalized to the value at 15 K for each pressure. The pressure dependence of the resistance at 15 K is shown in Fig. S1 in the Supplemental Materials. Initially, the T_c is suppressed rapidly with increasing pressure, consistent with previous measurements below 2.2 GPa.[38, 39] Here, we observe T_c eventually disappears at 4.0 GPa. The superconductivity in this region is so sensitive to pressure that the transition broadens and the resistance does not drop to zero even under 0.86 GPa. Figure 2b, c show the normalized resistance curves above 5.0 GPa. The drop of resistance re-emerges below 4.5 K at 5.0 GPa, implying the arise of another superconducting phase. This resistance drop exists in a wide pressure range from 5.0 to 22.3 GPa, and maximum T_c reaches 6 K, a 30% enhancement from the highest value in the first dome. With further increasing pressure, the resistance drop vanishes and the $R(T)$ curve exhibits a semiconducting behavior.

To make sure the resistance drop under high pressure represents a superconducting transition, we applied magnetic field to the low-temperature resistance measurements at 19.0 GPa. As shown in Fig. 2d, the resistance drop is gradually suppressed to lower temperature with increasing field, which demonstrates that it is indeed a superconducting transition. The inset of Fig. 2d plots the reduced temperature $T = T_c$ dependence of the upper critical field H_{c2}. The data can be fitted to the generalized Ginzburg–Landau model: $H_{c2}(T) = H_{c2}(0)\ (1-t^2)/(1+t^2)$, where $t = T/T_c$. According to the fit, $H_{c2}(0) \approx 0.81$ T is obtained.

Crystal structure evolution under pressure

In situ synchrotron powder XRD measurements were utilized to study the structural evolution of FeS with pressure. Figure 3a

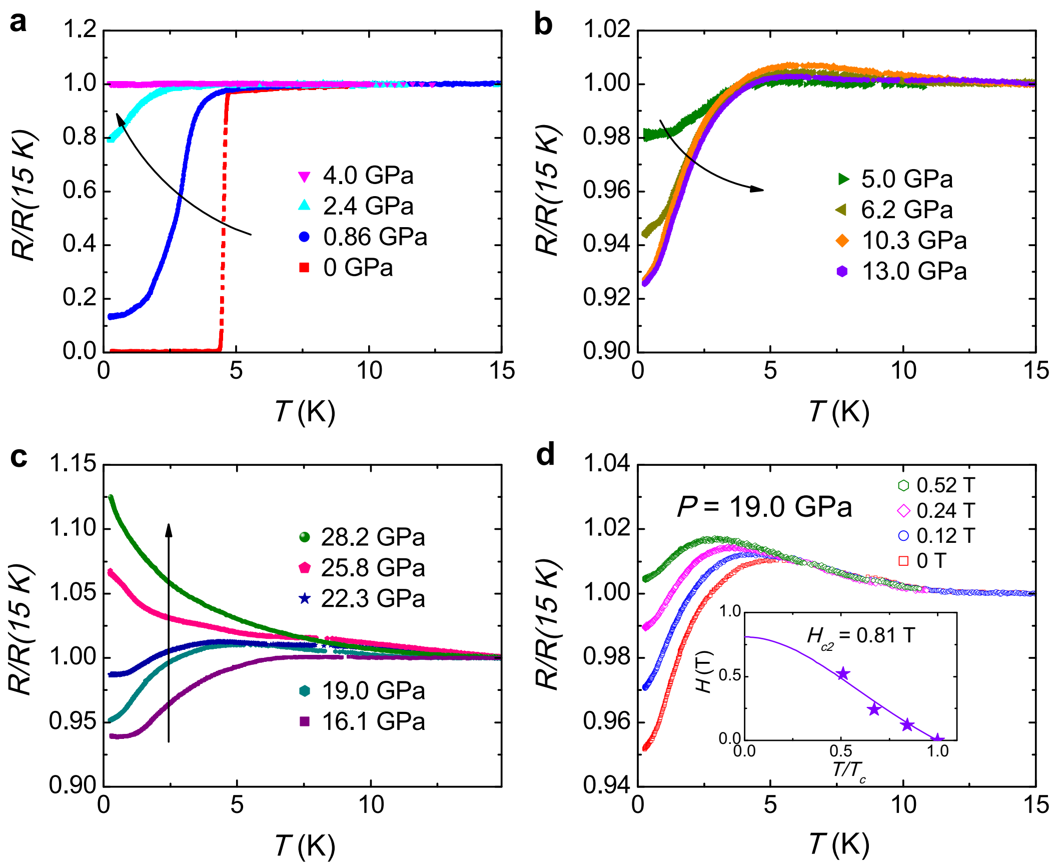

Fig. 2 **a–c** The normalized resistance curves of FeS single crystal under various pressures. **d** The superconducting transition of FeS at 19.0 GPa in various magnetic fields. The inset shows the reduced temperature ($T = T_c$) dependence of the upper critical field $H_{c2}(T)$. The solid line is a fit to the generalized Ginzburg–Landau model: $H_{c2}(T) = H_{c2}(0)\ (1 - t^2)/(1 + t^2)$, where $t = T/T_c$

displays the obtained XRD patterns under various pressures at room temperature. At the lowest pressure (1.0 GPa), the pattern can be well characterized as the tetragonal phase. From 7.2 to 9.2 GPa, a set of new peaks emerges with increasing intensity, while the intensity of the original peaks decreases. This indicates a structural transition and the coexistence of two different phases. The peaks from the low-pressure phase cannot be distinguished above 10.1 GPa, and the high-pressure phase remains stable up to 38.1 GPa.

On the basis of the Rietveld refinements, the low-pressure structure can be well indexed in the tetragonal space group *P4/nmm*, with the lattice parameters $a = 3.650$ Å and $c = 4.940$ Å at 1.0 GPa. Comparing to the ambient pressure FeS structure,[30] the values of a and c decrease slightly due to the shrinkage of lattices under pressure. On the high-pressure side, the hexagonal space group *P-62c* is found to be the optimal structure when we refine the XRD data above 10.1 GPa. The corresponding two crystal structures are shown in Fig. 3b, c, respectively. Similar pressure-induced structural transition from a tetragonal to hexagonal phase was also observed in FeSe, with a wide pressure range for two-phase co-existence.[5] The pressure dependence of the lattice parameters a, c, and unit cell volume is plotted in Fig. 3d–f, respectively. These lattice parameters show an abrupt change when the tetragonal structure transforms to the hexagonal one. The unit cell volume of the hexagonal phase is 13% smaller than that of the tetragonal phase at 7.2 GPa, which reveals the increase of the sample density, as expected.

Temperature–pressure phase diagram

We summarize our experimental results in Fig. 4. Figure 4a shows the pressure dependence of phase content around the structural transition. The hexagonal phase first appears ~7.2 GPa and its content increases rapidly with pressure. The original tetragonal phase occupies a small portion (~3%) at 9.2 GPa and is hardly distinguishable through the refinement above 10.1 GPa. The temperature–pressure (T–P) phase diagram is summarized in Fig. 4b. The superconductivity is rapidly suppressed by pressure in the first superconducting dome (SC-I), while it re-emerges in a wide pressure range from 5.0 to 22.3 GPa, manifesting as a second superconducting dome (SC-II) with a maximum T_c of 6.0 K around 16.1 GPa. Upon further compression, FeS remains the hexagonal structure and behaves as a semiconductor.

Since the two-phase (tetragonal + hexagonal) coexisting region (7.2–9.2 GPa) lies inside the second superconducting dome (5.0–22.3 GPa), we try to identify which phase is responsible for SC-II. Firstly, well inside the second dome, e.g., $P = 13.0$ and 16.1 GPa, the sample is dominated by the hexagonal phase, but the resistance drop is only a few percent. This suggests that the SC-II should not come from the major hexagonal phase. Secondly, all the IBSs have manifested superconductivity in either tetragonal or orthorhombic phase so far.[1–3] Thirdly, hexagonal FeS which has been extensively studied under high pressure, is in a NiAs-type structure at ambient pressure and transforms into a MnP-type structure at around 3 GPa. Upon further compression, it becomes a monoclinic structure at ~7 GPa and remains in this structure up to 40 GPa. In all the three structure, FeS shows semiconducting behavior and no superconductivity was reported.[31, 40, 41]

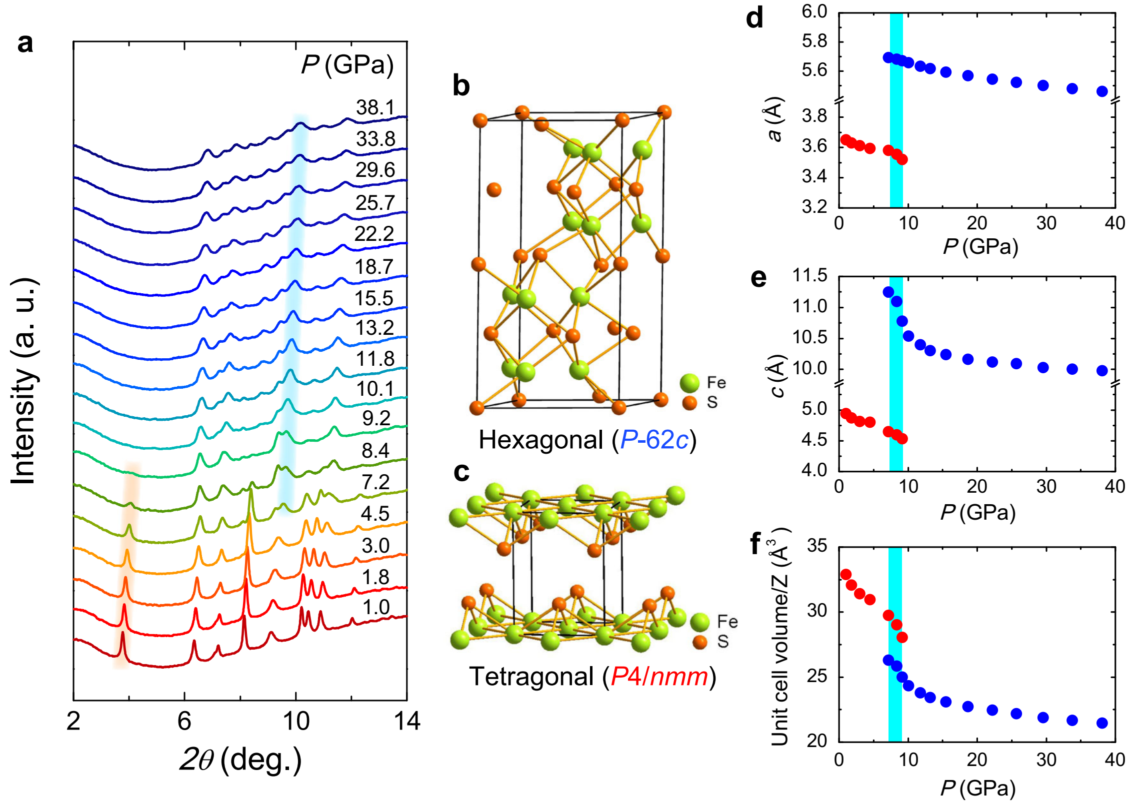

Fig. 3 **a** The *in situ* powder synchrotron XRD patterns of FeS under various pressures at room temperature. The characteristic peaks of two structures are marked to show the evolution with increasing pressure. **b**, **c** Net-like hexagonal structure (*P-62c*) and layered tetragonal structure (*P4/nmm*) of FeS. **d**–**f** Pressure dependence of the lattice parameters *a*, *c*, as well as unit cell volume. The red and blue solid circles represent the tetragonal and hexagonal phase, respectively. A two-phase coexisting region is highlighted from 7.2 to 9.2 GPa

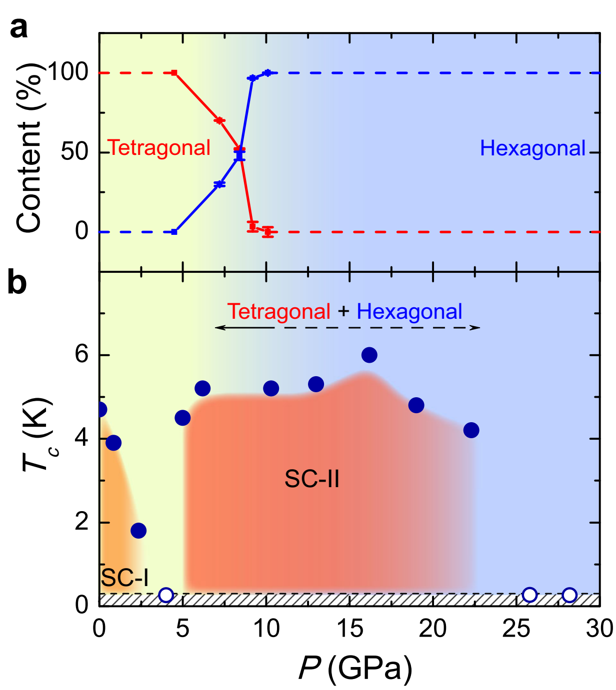

Fig. 4 **a** The pressure dependence of phase contents around the structure transition, which are obtained through refinements. **b** Temperature–pressure phase diagram of FeS. There are apparently two superconducting domes, and the second dome is attributed to the remaining tetragonal phase

Therefore, it is very likely that the SC-II arises from the remaining tetragonal phase of FeS, which coexists with the hexagonal phase up to ~22.3 GPa. For the XRD patterns with only a few percent of tetragonal phase, it is beyond the refinement capability to distinguish it from the major hexagonal phase, thus the Rietveld refinements beyond 10.1 GPa have ignored the contribution of tetragonal phase. We notice that previous studies suggested a close relationship between the structure of Fe_2X_2 layer and T_c in IBSs.[42–45] Thus we perform further analysis on the detailed crystal structure of tetragonal FeS up to 9.2 GPa (see the Supplemental Materials).

DISCUSSION

The two superconducting domes we observe here in FeS are quite different from that of its sister compound FeSe.[5] For FeSe, its *T*–*P* phase diagram has only one superconducting dome with the maximum $T_c = 36.7$ K at 8.9 GPa.[5] Since sulfur atom has a smaller radius than selenium atom, FeS can be considered as FeSe under chemical pressure. In this sense, the rapid T_c suppression in the first dome of FeS below 4 GPa may correspond to the high-pressure side of the superconducting dome observed in FeSe. However, so far, there is no report on the second superconducting dome in the *T*–*P* phase diagram of FeSe. The two domes in FeS are also different from the single dome observed in the *T* - *P* phase diagram of AFe_2As_2 (*A* = alkaline-earth metals) and *R*FeAsO (*R* = rare-earth metals).[46]

Previously, two superconducting domes in the *T*–*P* phase diagram were reported in two other IBS systems.[37, 47–51] For $(K/Tl/Rb)_xFe_{2-y}Se_2$, the T_c has a maximum value of 32 K at 1 GPa within the first dome, and a maximum T_c of 48.7 K in the second dome between 9.8 and 13.2 GPa.[37] The reason for this re-emergency of superconductivity under high pressure is still unknown. For KFe_2As_2, the T_c exhibits a V-shaped dependence under $P<3$ GPa, which was suggested as an indication of pairing symmetry change.[47–49] Similar behavior was also observed in $RbFe_2As_2$ and $CsFe_2As_2$.[50] Upon further compressing KFe_2As_2, a structural transition takes place from the tetragonal to collapsed tetragonal phase around 16 GPa, and a second superconducting dome with T_c greatly enhanced is observed.[51] However, Wang et al. later reported that the collapsed tetragonal KFe_2As_2 does not show superconducting behavior.[52] They claim that the previously reported observation of the superconducting transition in the collapsed tetragonal phase may originate from the pressure inhomogeneity.[52]

Except for pressure-induced two superconducting domes, changing the carrier density can also leads to two superconducting domes in IBSs.[53–55] In $LaFeAsO_{1-x}F_x$, a second superconducting dome without low-energy magnetic fluctuations was observed at $0.25\le x\le 0.75$, where the maximal T_c at $x_{opt}=0.5$–0.55 is even higher than that at $x\le 0.2$.[53] As for $LaFeAs(O_{1-x}H_x)$, with increasing x, two superconducting domes appear: the first between $0.05\le x\le 0.20$ with $T_{c\ opt}=26$ K, and the second between $0.20\le x\le 0.42$ with $T_{c\ opt}=36$ K.[54] Recent STM study showed the emergence of two disconnected superconducting domes in K dosed FeSe ultrathin films grown on SiC substrate.[55] Since we did not perform Hall effect measurement on FeS single crystal under pressure, it is not clear whether there is a dramatic carrier density change with pressure in FeS.

Furthermore, two superconducting domes coming from isovalent substitution in IBSs were also reported.[56–58] In $LaFe(As_{1-x}P_x)O$, the first superconducting dome appear at $0.2\le x\le 0.4$ while the second dome emerges at $x>0.7$.[56, 57] As for $(Ca_4Al_2O_6)Fe_2(As_{1-x}P_x)_2$, a nodeless superconducting phase lies between $0\le x\le 0.4$ while another nodal one is around $x=1$.[58]

Actually, a superconducting dome in T–P or T–x phase diagram has been commonly observed in unconventional superconductors, including heavy-fermion/cuprate/organic superconductors, and IBSs.[59] The superconducting dome is usually related to a quantum critical point (QCP) associated with antiferromagnetism, charge-density waves, spin-density waves, nematic correlations, or orbital currents.[59] For example, two distinct superconducting domes was observed in heavy-fermion superconductor $CeCu_2(Si_{1-x}Ge_x)_2$ under pressure, where the low-pressure dome is attributed to an antiferromagnetic QCP and the high-pressure dome is probably related to density fluctuations.[60] For IBSs, the first dome at low carrier density or low pressure may come from a magnetic QCP.[3] In the four above-mentioned IBSs ($LaFeAsO_{1-x}F_x$, $LaFeAs(O_{1-x}H_x)$, $LaFe(As_{1-x}P_x)O$, $(Ca_4Al_2O_6)Fe_2(As_{1-x}P_x)_2$), the first dome is associated with an antiferromagnetic order.[54, 56–58] In this work, however, FeS at ambient pressure is non-magnetic above T_c and we note that the normal-state resistance curve of FeS with P around 4 GPa is quite flat at low temperature, which does not show a non-Fermi liquid behavior. Therefore, it is not clear whether the first dome in FeS comes from a magnetic QCP.

For the second dome in heavily doped IBSs, for instance, $LaFeAs(O_{1-x}H_x)$, $LaFe(As_{1-x}P_x)O$ and $(Ca_4Al_2O_6)Fe_2(As_{1-x}P_x)_2$, it is associated with an antiferromagnetic phase,[54, 56–58] while in $LaFeAsO_{1-x}F_x$, the second superconducting dome is accompanied by a structural transition.[53] Very recently, the structural and electronic properties of FeS both at ambient condition and high pressure were theoretically studied by Tresca et al.[61] They claim a topological change of the Fermi surface as a function of the pressure in FeS,[61] which may be the origin of the observed second superconducting dome in our work.

In summary, we demonstrate two superconducting domes in the temperature–pressure phase diagram of the newly discovered superconductor FeS by means of high-pressure resistance measurements. The *in situ* high-pressure XRD results reveal a phase transition from pristine tetragonal to a hexagonal structure in a broad pressure range. The superconductivity in both domes originates from tetragonal FeS phase. The observation of two superconducting domes in FeS, together with similar results reported earlier in two other IBS systems, poses great challenges for understanding the pairing mechanism of IBSs.

METHODS

FeS single crystals were synthesized by de-intercalation of K from $K_{0.8}Fe_{1.6}S_2$ precursor by hydrothermal method.[62] XRD was carried out at room temperature using Bruker D8 Advance diffractometer (Cu K_α radiation, $\lambda=1.5408$ Å). Single crystal XRD of FeS was carried out on a Bruker SMART Apex (II) diffractometer (Mo K_α radiation, $\lambda=0.71073$ Å). Scanning electron microscopy (SEM) images were taken on an Electron Probe Microanalyzer (Shimadzu, EPMA-1720). The dc magnetization was measured in a Superconducting Quantum Interference Device (SQUID, Quantum Design). Electrical resistivity measurement at ambient pressure was performed in ^{4}He and ^{3}He cryostats, by a standard four-probe technique. For resistance measurement under pressure, a non-magnetic BeCu diamond anvil cell (DAC) was used to apply high pressure. To study the structure evolution of pressurized FeS, the *in situ* high-pressure powder angle-dispersive XRD (AD-XRD) experiment was performed at room temperature in a Micro XRD beamline (16-BM-D), High-Pressure Collaborative Access Team (HP-CAT), Advanced Photon Source, Argonne National Laboratory, using a monochromatic X-ray beam with the incident wavelength of 0.3263 Å. More experimental details can be found in the Supplemental Materials.

Data availability

The data supporting the findings of this study are available from the corresponding authors on reasonable request.

ACKNOWLEDGEMENTS

This work is supported by the Ministry of Science and Technology of China (Grant No. 2015CB921401, and 2016YFA0300503), the Natural Science Foundation of China (Grant No. 91421101, 11422429, 11421404, 51527801, U1530402), Program for Professor of Special Appointment (Eastern Scholar) at Shanghai Institutions of Higher Learning, and STCSM of China (No. 15XD1500200). W.Y. acknowledges the financial support from DOE-BES X-ray Scattering Core Program under grant number DE-FG02-99ER45775. We acknowledge Dr. Changyong Park for the assistance of beamline setup during the high-pressure XRD experiments. HPCAT operations are supported by DOE-NNSA under Award No. DE-NA0001974 and DOE-BES under Award No. DE-FG02- 99ER45775, with partial instrumentation funding by NSF. APS was supported by DOE-BES, under Contract No. DE-AC02-06CH11357.

AUTHOR CONTRIBUTIONS

T.P.Y. and Y.J.Y. grew the single crystals. J.Z., F.L.L., Y.X. and M.X.W. performed the high-pressure resistance measurements. J.Z., X.C.H. and L.P.H. analyzed the transport data. F.L.L. and W.G.Y. performed the high-pressure XRD measurements. F.L.L, N.N.L. and W.G.Y. analyzed the XRD data. J.Z., F.L.L., T.P.Y., W.G.Y. and S.Y.L. wrote the manuscript. S.Y.L. and W.G.Y. conceived and designed the project. All authors contributed to the discussion of the results and revision of the manuscript.

ADDITIONAL INFORMATION

Supplementary Information accompanies the paper on the *npj Quantum Materials* website (doi:10.1038/s41535-017-0050-7).

Competing interests: The authors declare no competing financial interests.

Publisher's note: Springer Nature remains neutral with regard to jurisdictional claims in published maps and institutional affiliations.

REFERENCES

1. Stewart, G. R. Superconductivity in iron compounds. *Rev. Mod. Phys.* **83**, 1589 (2011).
2. Chen, X. H., Dai, P. C., Feng, D. L., Xiang, T. & Zhang, F.-C. Iron-based high transition temperature superconductors. *Natl Sci. Rev.* **1**, 371–395 (2014).
3. Dai, P. C. Antiferromagnetic order and spin dynamics in iron-based superconductors. *Rev. Mod. Phys.* **87**, 855 (2015).

4. Hsu, F. C. et al. Superconductivity in the PbO-type structureα-FeSe. *Proc. Natl Acad. Sci. USA* **105**, 14262–14264 (2008).
5. Medvedev, S. et al. Electronic and magnetic phase diagram of β-$Fe_{1.01}Se$ with superconductivity at 36.7 K under pressure. *Nat. Mater.* **8**, 630–633 (2009).
6. Mizuguchi, Y., Tomioka, F., Tsuda, S., Yamaguchi, T. & Takano, Y. Superconductivity at 27 K in tetragonal FeSe under high pressure. *Appl. Phys. Lett.* **93**, 152505 (2008).
7. Miyata, Y., Nakayama, K., Sugawara, K., Sato, T. & Takahashi, T. High-temperature superconductivity in potassium-coated multilayer FeSe thin films. *Nat. Mater.* **14**, 775–779 (2015).
8. Lu, X. F. et al. Coexistence of superconductivity and antiferromagnetism in $(Li_{0.8}Fe_{0.2})$OHFeSe. *Nat. Mater.* **14**, 325–329 (2015).
9. Hanzawa, K., Sato, H., Hiramatsu, H., Kamiya, T. & Hosono, H. Field-induced superconducting transition at 31 K in insulating FeSe thin film. *Proc. Natl. Acad. Sci. USA* **113**, 3986 (2016).
10. Shiogai, J., Ito, Y., Mitsuhashi, T., Nojima, T. & Tsukazaki, A. Electric-field-induced superconductivity in electrochemically etched ultrathin FeSe films on $SrTiO_3$ and MgO. *Nat. Phys.* **12**, 42–46 (2016).
11. Lei, B. et al. Evolution of high-temperature superconductivity from low-T_c phase tuned by carrier concentration in FeSe thin flakes. *Phys. Rev. Lett.* **116**, 077002 (2016).
12. Wang, Q.-Y. et al. Interface-induced high-temperature superconductivity in single unit-cell FeSe films on $SrTiO_3$. *Chin. Phys. Lett.* **29**, 037402 (2012).
13. Liu, D. et al. Electronic origin of high-temperature superconductivity in single-layer FeSe superconductor. *Nat. Commun.* **3**, 931 (2012).
14. He, S. L. et al. Phase diagram and electronic indication of high-temperature superconductivity at 65K in single-layer FeSe films. *Nat. Mater.* **12**, 605–610 (2013).
15. Tan, S. Y. et al. Interface-induced superconductivity and strain-dependent spin density waves in FeSe/$SrTiO_3$ thin films. *Nat. Mater.* **12**, 634–640 (2013).
16. Peng, R. et al. Tuning the band structure and superconductivity in single-layer FeSe by interface engineering. *Nat. Commun.* **5**, 5044 (2014).
17. Ge, J.-F. et al. Superconductivity above 100 K in single-layer FeSe films on doped $SrTiO_3$. *Nat. Mater.* **14**, 285–289 (2015).
18. Lee, J. J. et al. Interfacial mode coupling as the origin of the enhancement of T_c in FeSe films on $SrTiO_3$. *Nature* **515**, 245–248 (2014).
19. Xie, Y., Cao, H. Y., Zhou, Y., Chen, S., Xiang, H. & Gong, X. G. Oxygen vacancy induced flat phonon mode at FeSe/$SrTiO_3$ interface. . *Sci. Rep.* **5**, 10011 (2015).
20. Nakayama, K. et al. Reconstruction of band structure induced by electronic nematicity in an FeSe superconductor. *Phys. Rev. Lett.* **113**, 237001 (2014).
21. Maletz, J. et al. Unusual band renormalization in the simplest iron-based superconductor $FeSe_{1-x}$. *Phys. Rev. B* **89**, 220506(R) (2014).
22. Watson, M. D. et al. Emergence of the nematic electronic state in FeSe. *Phys. Rev. B* **91**, 155106 (2015).
23. Zhang, P. et al. Observation of two distinct d_{xz}/d_{yz} band splittings in FeSe. *Phys. Rev. B* **91**, 214503 (2015).
24. Wen, C. H. P. et al. Anomalous correlation effects and unique phase diagram of electron-doped FeSe revealed by photoemission spectroscopy. *Nat. Commun.* **7**, 10840 (2016).
25. Miyata, Y., Nakayama, K., Sugawara, K., Sato, T. & Takahashi, T. High-temperature superconductivity in potassium-coated multilayer FeSe thin films. *Nat. Mater.* **14**, 775 (2015).
26. Niu, X. H. et al. Surface electronic structure and isotropic superconducting gap in $(Li_{0.8}Fe_{0.2})$ OHFeSe. *Phys. Rev. B* **92**, 060504 (2015).
27. Zhao, L. et al. Common electronic origin of superconductivity in (Li,Fe)OHFeSe bulk superconductor and single-layer FeSe/$SrTiO_3$ films. *Nat. Commun.* **7**, 10608 (2016).
28. Hanaguri, T. et al. Unconventional *s*-wave superconductivity in Fe(Se,Te). *Science* **328**, 474–476 (2010).
29. Fan, Q. et al. Plain *s*-wave superconductivity in single-layer FeSe on $SrTiO_3$ probed by scanning tunneling microscopy. *Nat. Phys.* **11**, 946–952 (2015).
30. Lai, X. et al. Observation of superconductivity in tetragonal FeS. *J. Am. Chem. Soc.* **137**, 10148–10151 (2015).
31. Ono, S. et al. High-pressure phase transformations of FeS: novel phases at conditions of planetary cores. *Earth Planet. Sci. Lett.* **272**, 481–487 (2008).
32. Zhang, L., Singh, D. J. & Du, M.-H. Density functional study of FeS, FeSe, and FeTe: Electronic structure, magnetism, phonons, and superconductivity. *Phys. Rev. B* **78**, 134514 (2008).
33. McQueen, T. M. et al. Extreme sensitivity of superconductivity to stoichiometry in $Fe_{1+\delta}Se$. *Phys. Rev. B* **79**, 014522 (2009).
34. Pachmayr, U., Fehn, N. & Johrendt, D. Structural transition and superconductivity in hydrothermally synthesized Fe*X* (*X*=S, Se). *Chem. Commun.* **52**, 194–197 (2016).
35. Ying, T. P. et al. Nodal superconductivity in FeS: evidence from quasiparticle heat transport. *Phys. Rev. B* **94**, 100504(R) (2016).
36. Xing, J. et al. Nodal superconducting gap in tetragonal FeS. *Phys. Rev. B* **93**, 104520 (2016).
37. Sun, L. et al. Re-emerging superconductivity at 48 kelvin in iron chalcogenides. *Nature* **483**, 67–69 (2012).
38. Borg, C. K. et al. Strong anisotropy in nearly ideal-tetrahedral superconducting FeS single crystals. *Phys. Rev. B* **93**, 094522 (2016).
39. Holenstein, S. et al. Coexistence of low moment magnetism and superconductivity in tetragonal FeS and suppression of T_c under pressure. *Phys. Rev. B* **93**, 140506 (2016).
40. Gosselin, J. R., Townsend, M. G. & Tremblay, R. J. Electric anomalies at the phase transition in FeS. *Solid State Commun.* **19**, 799–803 (1976).
41. Takele, S. & Hearne, G. R. Electrical transport, magnetism, and spin-state configurations of high-pressure phases of FeS. *Phys. Rev. B* **60**, 4401 (1999).
42. Lee, C.-H. et al. Effect of structural parameters on superconductivity in fluorine-free $LnFeAsO_{1-y}$(Ln=La, Nd). *J. Phys. Soc. Jpn.* **77**, 083704 (2008).
43. Horigane, K., Hiraka, H. & Ohoyama, K. Relationship between structure and superconductivity in $FeSe_{1-x}Te_x$. *J. Phys. Soc. Jpn.* **78**, 074718 (2009).
44. Margadonna, S. et al. Pressure evolution of the low-temperature crystal structure and bonding of the superconductor FeSe (T_c = 37 K). *Phys. Rev. B* **80**, 064506 (2009).
45. Tomita, T. et al. Correlation between T_c and crystal structure in s-doped FeSe superconductors under pressure: studied by x-ray diffraction of $FeSe_{0.8}S_{0.2}$ at low temperatures. *J. Phys. Soc. Jpn.* **84**, 84–93 (2015).
46. Sefat, A. S. Pressure effects on two superconducting iron-based families. *Rep. Prog. Phys.* **74**, 124502 (2011).
47. Tafti, F. F. et al. Sudden reversal in the pressure dependence of T_c in the iron-based superconductor KFe_2As_2. *Nat. Phys.* **9**, 349–352 (2013).
48. Taufour, V. et al. Upper critical field of KFe_2As_2 under pressure: a test for the change in the superconducting gap structure. *Phys. Rev. B* **89**, 220509(R) (2014).
49. Terashima, T. et al. Two distinct superconducting states in KFe_2As_2 under high pressure. *Phys. Rev. B* **89**, 134520 (2014).
50. Tafti, F. F. et al. Universal V-shaped temperature-pressure phase diagram in the iron-based superconductors KFe_2As_2, $RbFe_2As_2$, and $CsFe_2As_2$. *Phys. Rev. B* **91**, 054511 (2015).
51. Ying, J.-J. et al. Tripling the critical temperature of KFe_2As_2 by carrier switch. Preprint at http://arxiv.org/abs/1501.00330 (2015).
52. Wang, B. et al. Absence of superconductivity in the collapsed tetragonal phase of KFe_2As_2 under hydrostatic pressure. *Phys. Rev. B* **94**, 020502(R) (2016).
53. Yang, J. et al. New superconductivity dome in $LaFeAsO_{1-x}F_x$ accompanied by structural transition. *Chin. Phys. Lett.* **32**, 107401 (2015).
54. Hiraishi, M. et al. Bipartite magnetic parent phases in the iron oxypnictide superconductor. *Nat. Phys.* **10**, 300 (2014).
55. Song, C. L. et al. Observation of double-dome superconductivity in potassium-doped FeSe thin films. *Phys. Rev. Lett.* **116**, 157001 (2016).
56. Shiota, T. et al. Multiple antiferromagnetic spin fluctuations and novel evolution of T_c in iron-based superconductors $LaFe(As_{1-x}P_x)(O_{1-y}F_y)$ revealed by ^{31}P-NMR studies. *J. Phys. Soc. Jpn.* **85**, 053706 (2016).
57. Mukuda, H. et al. Emergence of novel antiferromagnetic order intervening between two superconducting phases in $LaFe(As_{1-x}P_x)O$: ^{31}P-NMR studies. *J. Phys. Soc. Jpn.* **83**, 083702 (2014).
58. Kinouchi, H. et al. Emergent phases of nodeless and nodal superconductivity separated by antiferromagnetic order in iron-based superconductor $(Ca_4Al_2O_6)Fe_2(As_{1-x}P_x)_2$: ^{75}As- and ^{31}P-NMR studies. *Phys. Rev. B* **87**, 121101(R) (2013).
59. Norman, M. R. The challenge of unconventional superconductivity. *Science* **332**, 196 (2011).
60. Yuan, H. Q. et al. Observation of two distinct superconducting phases in $CeCu_2Si_2$. *Science* **302**, 5653 (2003).
61. Tresca, C., Giovannetti, G., Capone, M. & Profeta, G. Electronic properties of superconducting FeS. *Phys. Rev. B* **95**, 205117 (2017).
62. Lin, H. et al. Multi-band superconductivity and large anisotropy in FeS crystals. *Phys. Rev. B* **93**, 144505 (2016).